Pergamon

Geochimica et Cosmochimica Acta, Vol. 65, No. 7, pp. 1047–1057, 2000

0016-7037/00 $20.00 + .00

PII S0016-7037(00)00542-1

Conformations and aggregate structures of sorbed natural organic matter on muscovite and hematite

KSENIJA NAMJESNIK-DEJANOVIC[1] and PATRICIA A. MAURICE[2,*]

[1] Department of Geology, Kent State University, Kent, OH 44242 USA
[2] Dept. of Civil Engineering and Geological Sciences, University of Notre Dame, Notre Dame, IN 46556, USA

(*Received October* 11, 1999; *accepted in revised form August* 4, 2000)

Abstract—In-solution atomic-force microscopy was used to characterize molecular dimensions and aggregate structures of natural organic matter (NOM) sorbed to the basal-plane surfaces of muscovite and hematite as a function of pH (3–11), ionic strength (0.001–0.3 M), NOM concentration (20–100 mgC L^{-1}), and cation electrolyte identity (Ca, Na, Li added as Cl-salts). Electrolyte identity and concentration exerted important effects on image stability, particle size, and sorption density. On mica, the presence of either Ca^{2+} or Li^{+} led to more stable images than Na^{+}. For example, at pH 3, we were unable to obtain stable images of NOM on mica in NaCl. However, at pH 3 in $CaCl_2$ and LiCl solutions, we observed adsorbed spheres with diameters appropriate for single molecules. A higher apparent adsorption density was observed in $CaCl_2$ than in LiCl, consistent with previous reports that Ca enhances NOM adsorption. In LiCl, the spheres often were aggregated into small groups whereas in $CaCl_2$, they were mostly isolated.

At intermediate pH and relatively low NOM concentrations on mica, larger spherical aggregates were observed, but at higher NOM concentrations, we observed ring structures with nanoporosity that could be important for partitioning of organic pollutants. At high pH on mica, we observed an highly ordered array which most probably indicates reordering of the mica surface structure as Si released by dissolution interacts with NOM. This indicates that NOM may play an important role in phyllosilicate diagenesis. On hematite at pH 4 and in the presence of high dissolved iron concentration, large spherical NOM aggregates were observed, consistent with observations by Myneni et al. (1999) using in solution X-ray imaging. Overall our results demonstrate that NOM sorbs in complex structures and aggregates. Therefore, current models of NOM sorption are likely overly simplistic and require further direct verification. *Copyright © 2000 Elsevier Science Ltd*

1. INTRODUCTION

Natural organic matter (NOM) is ubiquitous throughout aquatic and terrestrial ecosystems, and decades of research have greatly increased our understanding of its chemical composition, structure, and reactivity. Nevertheless, for complex NOM components such as the humic and fulvic acids (HA and FA, respectively), we still know relatively little about the structure(s) and configurations of individual molecules and the physicochemical characteristics of aggregates, particularly when sorbed to mineral surfaces. Yet, such information is of fundamental importance for developing realistic models of NOM interactions with pollutants, especially with respect to partitioning of hydrophobic organic compounds (HOCs) (McCarthy and Jimenez, 1985; Murphy, et al., 1990; Schlautman and Morgan, 1993; Murphy et al., 1994; Piatt and Brusseau, 1998; Pignatello, 1998). Note that in this manuscript we use the term 'sorption' to include both adsorption (2-dimensional) and precipitation (3-dimensional).

Previous in-air atomic force microscopy (AFM; also known as scanning force microscopy, SFM) (Namjesnik-Dejanovic and Maurice, 1997; Mertig et al., 1999) showed results similar to those obtained by scanning electron microscopy (SEM) and transmission electron microscopy (TEM) (Stevenson and Schnitzer, 1982; Chen and Schnitzer, 1989; Leppard et al., 1990), but drying-induced artifacts most probably were present in the images.

This study expands upon our preliminary in-solution AFM analysis at high NOM concentration and pH ~5 (Maurice and Namjesnik-Dejanovic, 1999). That preliminary research showed ring-shaped aggregates. In our new research, we demonstrate that differing solution conditions (NOM concentration; pH 3–11; ionic strength 0.001–0.3 mol/L; cation counterion identity, Na^{+}, Li^{+}, Ca^{2+}; presence of trivalent cations, Fe^{3+}, Al^{3+}) and mineral surface properties (muscovite mica versus natural specular hematite) influence sorbed NOM configurations. Our research demonstrates that sorbed NOM may have complex aggregate structures. Further research clearly is needed to determine the controls on aggregate structures and the effects of different structures on the reactivity of sorbed NOM.

Currently, in-solution AFM does not provide resolution adequate to determine NOM molecular structure; e.g., identification of individual aromatic rings and aliphatic chains. However, we were able to image adsorbed particles with dimensions close to those reported previously for single molecules, based on results of small angle X-ray scattering (Aiken et al., 1994) and field flow fractionation (Schimpf and Petteys, 1996).

2. MATERIAL AND METHODS

2.1. NOM

The NOM samples were collected as part of an integrated study (1995–1999) of NOM evolution through a small freshwater wetland,

*Author to whom correspondence should be addressed (pmaurice@nd.edu).

Table 1. Summary of chemical characteristics of surface and shallow ground water at the sampling site, McDonalds Branch basin in the New Jersey Pine Barrens.

Site	pH	Conductance μS cm^{-1}	DOC mg L^{-1}	Fe μg L^{-1}	Al μg L^{-1}
		Typical range[a]			
Surface water (S-2)	3.2–4.2	60–440	5.6–37	360–4700	550–10000
Shallow (5.5 ft. deep) ground water (QWH-1A)	3.4–4.1	66–268	13–30	320–5000	880–5200
		Waters collected for this study			
Surface water (S-2)	3.8	91	24	523	709
Shallow (5.5 ft. deep) ground water (QWH-1A)	3.9	80	27	1061	1295

[a] Data from Lord et al. (1990).

McDonalds Branch basin in the Pine Barrens region of the New Jersey coastal plain (USA). The study site is described in detail elsewhere (Lord et al., 1990; Johnsson and Barringer, 1993; Meier et al., 1999). Briefly, it is an excellent location for NOM investigations because the low dissolved solids concentrations and wetland conditions permit accumulation of NOM in surface and shallow ground waters. Surface (site S-2; Lord et al., 1990) and shallow ground water (from a well in the stream channel, 5.5 ft. deep, QWH-1A; Lord et al., 1990) were collected from an upstream potential ground-water recharge area (actual recharge obstructed by a clay lens which underlies the stream at ~6 ft. deep) which has high NOM, low pH, low specific conductance indicating low ionic strength, and relatively high Al and Fe concentrations (See Table 1). Water samples were filtered through three consecutive filter cartridges with nominal pore sizes 20 μm, 1 μm, and 0.4 μm respectively, and refrigerated in the dark before use.

Humic substances (HS) were isolated from some samples using an ion-exchange resin procedure (XAD-8, Aiken et al., 1992). Some of the resulting isolates were freeze-dried and later redissolved in ultraviolet treated MilliQ deionized water for a minimum of 24 h. before use. Other samples were stored in dissolved form in a refrigerator for several months. Comparison of AFM images from samples that were never freeze dried with those which were freeze dried but redissolved showed no obvious effects of the freeze drying process on sorbed NOM configurations. In addition, a core was taken by hand auger of a muck deposit underlying the stream in the sampling area. HS were extracted with NaOH, isolated using XAD-8 resins (Aiken et al., 1992), and separated into HA and FA by acidification to pH < 2 and centrifugation (work performed by P. Maurice in USGS laboratories of G. Aiken and J. Leenheer). Weight average molecular weight (M_w) was determined using high pressure size exclusion chromatography (HPSEC) in the method of Chin et al. (1994) as revised by Zhou et al. (in press). Uncertainty of M_w measurements is estimated to be $\pm$ 100 Da (Zhou et al., 2000). Absorptivity normalized to mole C was calculated from absorbance at 280 nm using a double beam Hitachi U2000 spectrometer. M_w and absorptivity per mole of carbon were determined to be 2244 Da and 460 L/mol-C-cm for surface water XAD-8 extract; 2563 Da and 600 L/mol-C-cm for muck fulvic acid; and 2016 Da and 374 L/mol-C-cm for shallow ground water NOM.

2.2. Mineralogic Samples

AFM imaging of NOM requires sorption to a substrate. We chose muscovite mica from an unknown locality and natural specular hematite from Minas Gerais (Brazil) as the sorbents. Both surfaces have been widely studied using AFM (e.g., Johnsson et al., 1991; 1992; Maurice et al., 1995), and we have significant experience regarding potential AFM artifacts (Namjesnik-Dejanovic and Maurice, 1997; Maurice and Lower, 1998). Mica is the most commonly used substrate for AFM because its freshly cleaved basal-plane surfaces generally contain μm-scale molecularly flat regions. A drawback is that NOM sorbs relatively weakly to the basal-plane surface, even when electrolytes are added to enhance sorption (Dempsey and O'Melia, 1983).

The specular hematite could be fractured to produce fresh basal-plane surfaces that were fairly flat on the μm scale (Johnsson et al., 1991; Maurice et al., 1995). We cleaned the freshly fractured specimens in acetone for several minutes, then rinsed with ethanol and MilliQ water. Samples were air dried under protective cover to avoid contamination from air dust particles.

2.3. Electrolytes

In addition to pH, electrolytes strongly influence the sizes and conformations of macromolecules in solution (Cornel et al., 1986; Yokoyama et al., 1989; Schimpf and Petteys,1996; Stumm and Morgan, 1996). Electrolyte concentration and identity also control AFM image stability (Ducker et al., 1992). Electrolytes anchor molecules to the substrate, especially when a multivalent cation is used (Bezanilla et al., 1993; Hansma et al., 1994). We found that the stabilities of AFM images of NOM in Cl-salt electrolytes decreased in the order: $Ca^{2+} > Li^{+} > Na^{+}$. Samples of unaltered shallow groundwater used in our experiments (Table 1) naturally contain high concentrations of Al (1.5 ppm) and Fe (1.2 ppm). NOM from these samples could be imaged without addition of an electrolyte solution.

Table 2 contains a summary of the solution conditions (dissolved organic carbon concentration, DOC; pH; and electrolyte identity and concentration), the mineral substrate, and the observed results for each of the successful experiments described in detail below. DOC was measured using a Shimadzu TOC5000 carbon analyzer. The precision of analyses, as measured by relative standard deviation, was <2 to 5%. Because the volume of the AFM fluid cell is insufficient for postsorption analysis we cannot determine (by subtraction) the amount sorbed, and thus, report only the DOC concentration of solution injected into the fluid cell.

2.4. AFM Imaging Techniques

A Digital Instruments Nanoscope III AFM with an extender module for phase imaging was used in these experiments. We used tapping mode AFM (TMAFM; Frommer, 1992; Putman et al., 1994; Magonov and Reneker, 1997) throughout. In TMAFM, the probe intermittently taps the sample surface, minimizing lateral frictional forces during scanning and hence reducing the probability of damage of soft and easily deformable materials. However, TMAFM does not provide atomic-scale resolution.

A description of the AFM fluid cell is provided elsewhere (e.g., Maurice et al., 1995; Maurice and Lower, 1998) and the cell is shown schematically in Figure 1. It consists of three separate parts: a top made of glass, a bottom which is the sample attached to the substrate, and an *o*-ring between the two. The volume of the fluid cell is ~1 mL or less.

Mica samples were freshly cleaved as described by Namjesnik-Dejanovic and Maurice (1997). For some images, we placed a few drops of NOM solution onto a mica surface, allowed it to partially dry under protective cover for several hrs, attached the still damp sample to a steel AFM stub using double-sided tape, and then imaged in either electrolyte or an NOM/electrolyte solution. For other images, a freshly cleaved sample of mica was placed in the fluid cell, the surface was

Table 2. Summary of experimental conditions and results for samples described in detail herein.

Sample	pH, electrolyte conditions, and NOM concentration	Adsorbed NOM shape	Mean x-y (mm, ± STD)	Mean height (nm, STD)	Substrate
Surface water	pH 30.1 M LiCl, 25 mgC/L	Sphere	3.4 ± 1.0	0.6 ± 0.2	Muscovite
		Aggregates of spheres	12.2 ± 3.3	0.6 ± 0.2	
XAD-8 extract	pH 3, 0.001 M $CaCl_2$, 20–100 mgC/L	Sphere	1.9 ± 0.8	1.3 ± 0.7	
	pH 5, 0.1M $CaCl_2$, <100 mgC/L	Ring-shaped aggregates	49 ± 10[a]	3.5 ± 1.7[a]	
	pH 6, 0.03M $CaCl_2$, 75 mgC/L	Oblate-spherical aggregates	78 ± 13 (shortest crossection)	3.9 ± 1.4	
	pH 8, 0.001M $CaCl_2$, 100 mgC/L	Linear aggregates	53 ± 21 Width	1.5 ± 0.6	
Muck fulvic acid	pH 11 adjusted with NaOH, no additional electrolytes, 50 mgC/L	Fine-linear features	6.4 ± 1.9 Width	0.25 ± 0.1	Muscovite
Shallow ground water NOM	pH 4, no electrolyte added (naturally high Fe and Al[c]), 27 mgC/L	Globular or toroidal aggregates	300–1000	[b]	Hematite

[a] Maurice, P.A. and N-Dejanovic, K., 1999.
[b] Height undetermined; see text.
[c] See Table 1 for concentrations.

imaged in MilliQ water or electrolyte solution to determine surface microtopography in the absence of NOM, and an NOM-containing solution was then injected. AFM imaging commenced after ~2 h of sorption. In all cases, because the AFM o-ring sat atop the mica specimen, the AFM stub and tape did not come into contact with the solution.

Cleaned hematite samples were fixed on cleaned glass slides using an epoxy glue, and the glass slide mounted on a steel AFM stub using double-sided tape. Because the AFM fluid cell rested atop the glass slide, neither the tape nor the metal stub were in contact with the fluid-cell solution. Although the hematite basal-plane surface is not nearly as flat as muscovite (Johnsson et al., 1991; Junta and Hochella, 1994), NOM tends to sorb strongly to hematite (Tipping, 1981; Gu et al., 1994), facilitating AFM imaging. We first imaged the hematite surface in deionized water, then injected NOM-containing solution, allowed 2 h for sorption, and commenced AFM imaging. Some AFM experiments were performed over the course of 2 to 3 d. In such cases, the fluid cell was periodically slowly flushed with more of the same solution, and a 2-h sorption 'equilibration' time was allowed.

Height, amplitude, and phase-mode AFM images were collected simultaneously. Height mode images provide data in 3 dimensions and were used for all height (z-direction) measurements. Amplitude-mode images are similar, but they provide essentially the first derivative of the height. Edges are thus accentuated in the amplitude mode images. Particle widths were measured on amplitude-mode images. Most images shown here are amplitude-mode. In phase imaging, the phase lag of the cantilever oscillation, relative to the signal sent to the cantilever's piezo driver, is monitored (Radmacher et al., 1992; Magonov et al., 1997a,b; Babcock and Prater, 1991). The phase lag is highly sensitive to variations in material properties such as adhesion and viscoelasticity. Magonov et al., (1997a,b) showed that differences can occur in height and phase image quality and reproducibility by simply changing the ratio between the AFM's drive amplitude (the drive signal applied to the cantilever oscillator) and the set point (the parameter that defines the amplitude of the cantilever oscillation signal to be maintained by the feedback loop). This leads to so called hard, intermediate and/or light tapping conditions.

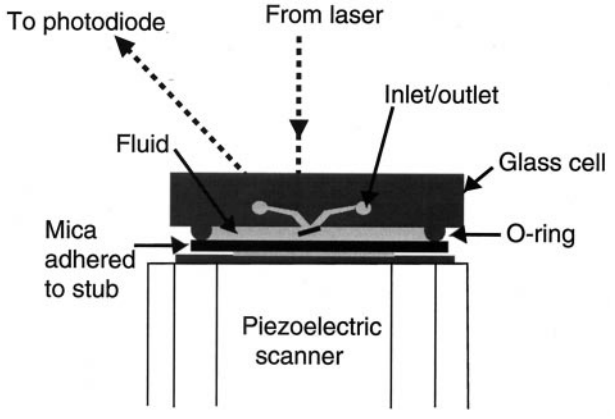

Fig. 1. Schematic illustration of the AFM fluid cell. Adapted from Maurice and Lower, 1998.

Our experience suggests that when imaging in solution, the quality of all three images (height, amplitude and phase) depends on the tapping conditions. Phase imaging was important because it provided independent verification of whether we were imaging NOM (less stiff) or substrate material (more stiff and harder material that causes larger phase shifts and thus appears brighter under the imaging conditions we used). An example of simultaneously collected amplitude- and phase-mode images of NOM on hematite is shown in Figure 2. With the tapping conditions employed, dark indicates higher local adhesive forces (between the sample and the tip) (Magonov et al., 1997b) of particles over the lighter background of less adhesive hematite. The differences in phase contrast thus verify the imaging of NOM on a hematite substrate.

Three types of probes were used: standard silicon nitride (Si_3N_4) contact mode tips (which also work well for TMAFM in solution); and silicon (Si) probes with cantilever lengths of 125 and 225 μm and resonant frequencies of 298 to 355 kHz and 67 to 94 kHz, respectively. (See http://www.di.com, under Tesp probes for detailed descriptions of tips). When working in solution, the cantilever resonance is largely damped and regardless of the type of cantilever employed, this resonance attenuation necessitates an increase of drive amplitude relative to what is used in air. The drawback is that the higher the drive amplitude, the more vigorously the probe vibrates and the more likely it is to result in damage and/or destruction of soft samples. We determined that the best NOM images could be obtained at drive amplitudes ~ 500 mV and should not exceed 1 V. The short (100 μm) thin-legged Si_3N_4 probes (nominal spring constant = 0.32 Nm^{-1}) performed the best. Although the manufacturer (Digital Instruments Manual) (Digital Instruments Inc., 1996–97) recommends resonance frequencies ~10 kHz, we obtained the best results with 27–33 kHz, regardless of probe type. Scan rate was ≤1 Hz.

Images were minimally processed ('flatten' and lowpass filtering; Digital Instruments Manual. Digital Instruments Inc., 1996–97) to prevent introduction of artifacts. In measuring dimensions of features, several nonideal properties of the microscope require special attention.

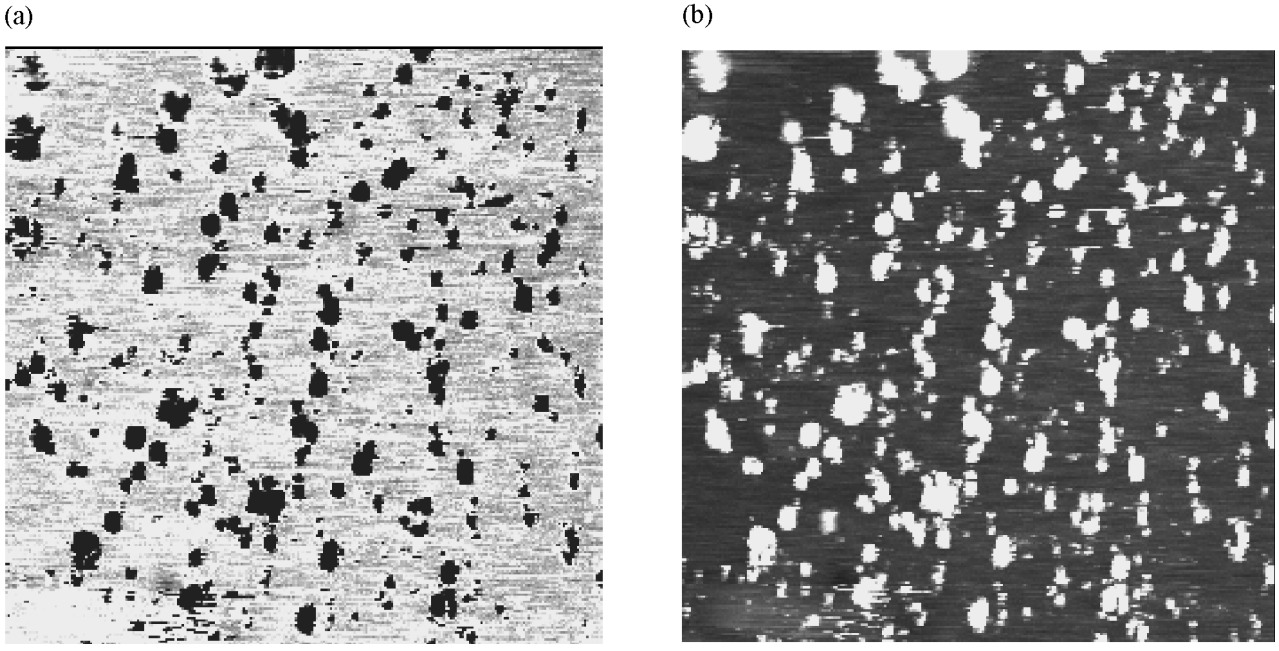

Fig. 2. Phase (left) and amplitude (right) mode images in solution of groundwater NOM on hematite. These and other images were collected using TMAFM. Images are 5.10 μm on a side. This figure demonstrates that phase imaging can be important for verifying that structures are likely NOM, with different viscoelastic properties from the substrate

First, there is an error in all measurements (x, y, z) caused by the nonlinear response, hysteresis, and creep of the piezoelectric scanner (Barrett and Quate, 1991; Digital Instruments Manual, Digital Instruments Inc., 1996–97). The Nanoscope III compensates for most of the piezoelectric scanner error. A much larger error is introduced by the finite shape and size of the probe, which ultimately leads to lateral enlargement of imaged particles. When compared to the probe error, the scanner error is usually ignored and the heights (z) of particles are considered to be much more accurate than the lateral (x-y) dimensions. In some cases, accuracy of lateral dimension measurements can be limited by pixel size in AFM images. All of the images shown here were collected at 512 $\times$ 512 pixel density. For soft and easily deformable NOM particles, scan areas of no less than ~400 to 500 nm on a side often were required because smaller scan sizes resulted in damage to the sample surface (see examples below); this is a common observation in our laboratory when dealing with soft materials. Therefore, some small features, such as single NOM molecules, were of dimensions (1–2 nm) comparable to the pixel size, which could result in an approximate 100% or more error for some particles.

A number of researchers have proposed methods to improve images by compensating for the probe error (Markiewicz and Goh, 1994; Butt and Gerharz, 1995; Siedlecki et al., 1996; Wilson et al., 1996; Maurice and Lower, 1998). However, current methods are hampered by the assumption that the probe geometry does not change through the imaging process. It is well known that probes become less sharp and image resolution deteriorates over time. Organic contaminants can be picked up by the probe, resulting in reduced resolution as well as multiple-tip artifacts (Barrett and Quate, 1991; Maurice et al., 1995; Namjesnik-Dejanovic and Maurice, 1997). With experience, such artifacts can be recognized and affected images discarded. We believe that features observed with different probes on numerous images using different scan angles are for the most part 'real' and do not need to be processed because the software can correct some errors but introduce others. The lateral width measurements reported in this paper (e.g., Table 2) should be considered as rough estimates of horizontal particle dimensions with the understanding that they can be overestimated by more than 100% in worse-case scenarios (e.g., Wilson et al., 1996; Maurice and Namjesnik-Dejanovic, 1999), although often much less than this.

3. RESULTS AND DISCUSSION

3.1. Imaging on Mica

AFM imaging of NOM in solution is extremely difficult. We tested a variety of sample preparation techniques, combinations of electrolytes (types and concentrations), pHs, NOM concentrations, substrates, AFM probes, and imaging parameters. Only some of them gave reproducible images. It appears that at least 2-h sorption 'equilibration' time is needed to obtain stable images. A similar sorption 'equilibration' time was observed from macroscopic NOM sorption experiments on goethite and kaolinite, in which both total sorbed NOM and NOM molecular weight were measured over time (Zhou et al., 2000; Namjesnik-Dejanovic et al., 2000). We provide examples of reproducible images, below.

Figure 3 is an example of structures observed on mica in a solution containing XAD-8 extract of surface water NOM (25 mg C L^{-1}) with 0.1 mol/L LiCl at pH = 3. In this image, the flat background is the mica surface. Flattened spherical particles, which we believe to be adsorbed NOM (they were absent when imaging in NOM-free solution), have lateral diameter (x-y dimension) from 1.9–15 nm and height (z-dimension) from 0.4 to 0.9 nm, with a mean of 0.6 nm. We believe that the smaller particles (lateral diameter 1.9–4.6 nm, mean 3.4 nm) are likely single molecules (see comparison with other methods, below), and that most of the larger and more irregularly shaped particles are aggregates of several smaller molecules; indeed, many appear to consist of 2 to 4 smaller flattened spherical structures linked together. Repeated imaging at the same site caused a decrease in the number of NOM particles present, suggesting that the probe can easily move what must be relatively weakly attached NOM.

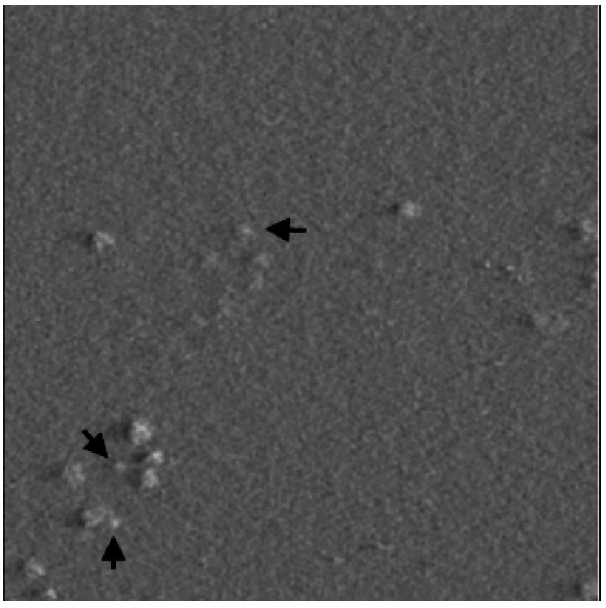

Fig. 3. Amplitude mode image of surface water XAD-8 isolate on muscovite in 0.1 mol/L LiCl at pH 3. Arrows point to spherical structures that are likely single molecules. 364 nm on a side.

Figure 4a,b shows structures observed for the same NOM sample, concentration, and initial pH but with 0.001 mol/L $CaCl_2$ used as a background electrolyte. In these images, the NOM appears as small spheres of uniform size, with lateral diameters between 0.8 and 3.0 nm, mean 1.9 nm; and height 0.4–2.5 nm, mean 1.3 nm. The spheres are more numerous per unit muscovite surface area and somewhat better resist repeated probe scanning, suggesting stronger adsorption to the muscovite surface in the presence of $CaCl_2$. However, the removal of adsorbed spheres with consecutive scans is obvious when consecutive scans Figure 4a,b are compared.

Comparison of particle dimensions measured in the two electrolytes suggests that the NOM consists of denser spherical-shaped structures in $CaCl_2$ than in LiCl solution, even at $CaCl_2$ concentrations 10 times lower than LiCl. In 0.05 and 0.1 mol/L NaCl solution, some scattered spheres were observed, but the images tended to be more noisy so that measurements could not be made accurately. In LiCl, 0.1 mol/L electrolyte concentration was needed to obtain stable images. For $CaCl_2$ concentrations ranging from 0.001–0.01 mol/L, we observed no difference in abundance, size or shape of imaged structures. We did not investigate higher or lower concentrations.

Keeping in mind that the x-y dimension is likely overestimated due to the finite radius of curvature of the AFM tip, and that height measurements also can be distorted, sizes measured in Figures 3 and 4 compare reasonably well with radius of gyration measurements obtained by previous researchers using X-ray scattering; 0.75 nm (=1.5 nm diameter) reported for Suwannee River fulvic acid and 1.13 nm (=2.26 nm diameter) for Suwannee River humic acid (Aiken et al., 1994). This suggests that the particles shown in Figures 3 to 4 generally represent single molecules of NOM, although as noted above, some of the larger particles in Figure 3 appear to be clusters of several individual molecules. Our results also agree with estimates by field flow fractionation for soil humic acid, Suwannee River fulvic acid, and a leaf leachate, which are in the range 0.5–3.0 nm (Schimpf and Petteys, 1996).

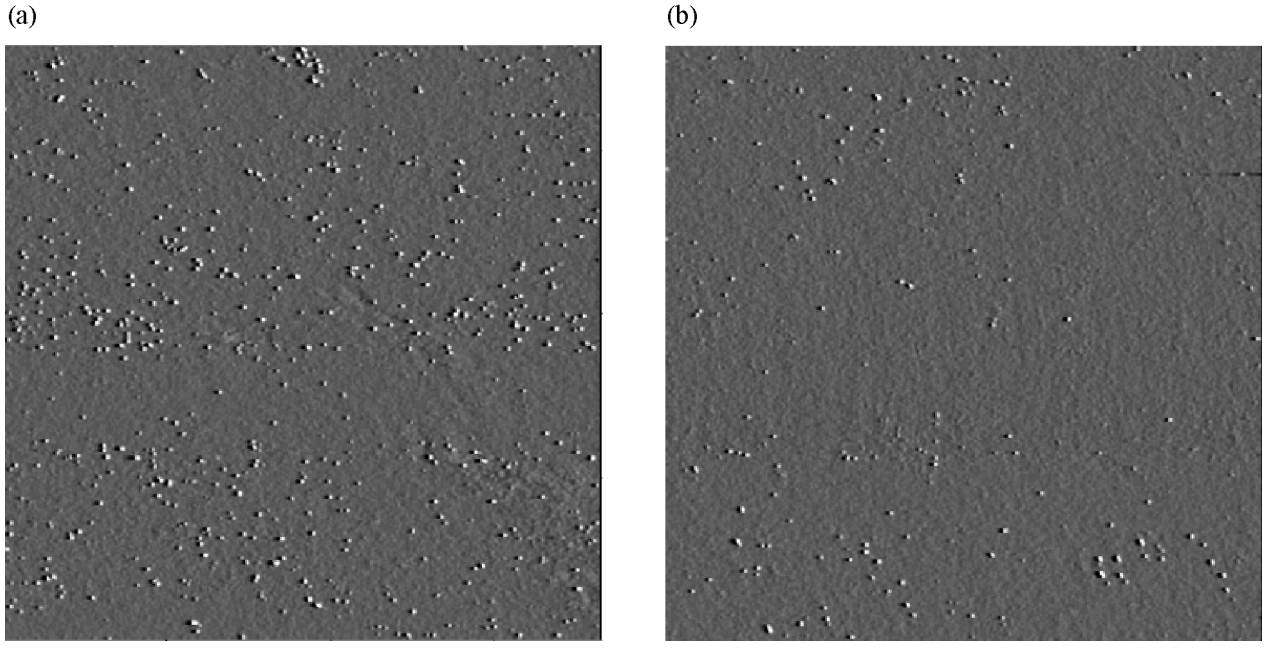

Fig. 4. Amplitude mode image of surface water XAD-8 isolate on muscovite in 0.001 mol/L $CaCl_2$ at pH 3. 392 nm on a side. Consecutive scans show higher adsorption density in earlier scan, figure (a) compared to later scan, (b), suggesting that the tip sweeps away NOM during scanning. Also, note that adsorption density in $CaCl_2$ is higher than in LiCl (Fig. 3) which is consistent with previous reports that Ca^{2+} strongly promotes NOM adsorption.

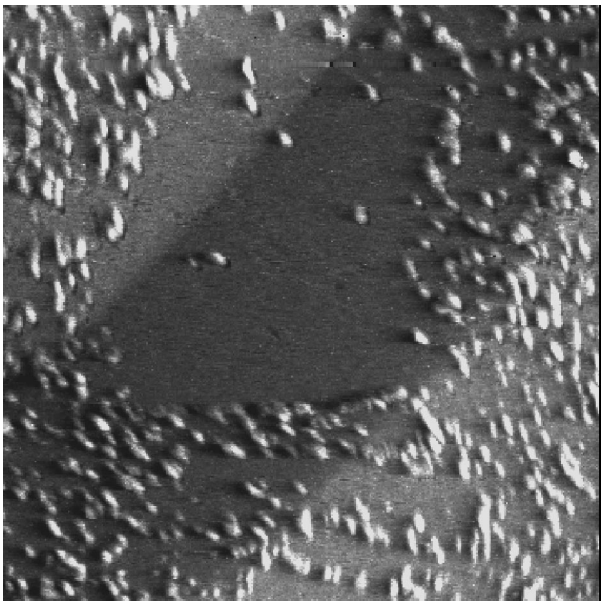

Fig. 5. Amplitude mode image of surface water XAD-8 isolate on muscovite in 0.03 mol/L $CaCl_2$ at pH 6. NOM was dislodged from the middle portion of this image during previous higher-resolution scanning. 5 μm on a side.

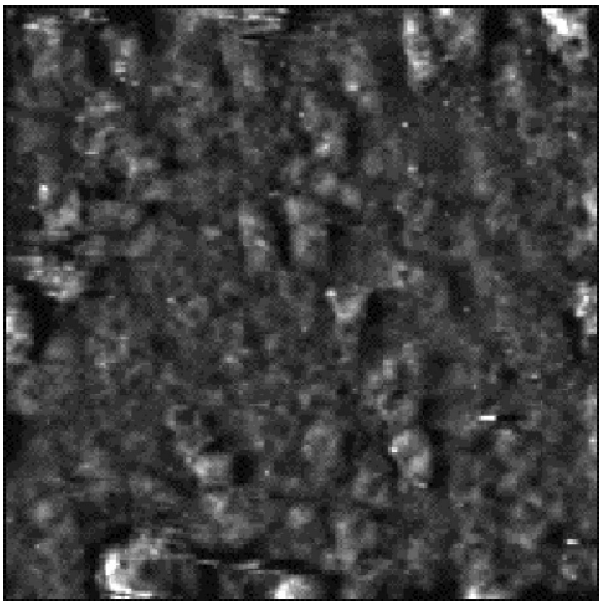

Fig. 6. Amplitude mode image of ~100 mgC L^{-1} surface water XAD-8 isolate on muscovite in 0.01 mol/L $CaCl_2$ at pH 5. 1.4 μm on a side. Re-printed by permission from *Env. Sci. Technol.*

We were unable to obtain stable images of NOM in NaCl solutions (0.001–0.1 mol/L) at pH 3. Some scattered spheres were observed, but they were easily swept away by the AFM tip. Yet, we were able to obtain stable images in $CaCl_2$ and LiCl. It has long been known that Ca^{2+} promotes NOM sorption relative to Na^+ (e.g., Tipping, 1981; Dempsey and O'Melia, 1983), which may explain the difference in image stability. Despite the low atomic weight of Li, Li^+ has a larger effective ionic radius than does Na^+ (Langmuir, 1997 and references therein). Hence, further investigation of the effects of Li^+ on NOM sorption are needed.

At pH 6, in 0.03 mol/L $CaCal_2$ and ~50 mgC L^{-1}, fairly uniform aggregates are observed that are somewhat elongated possibly due to scanner piezoelectric or thermal drift (Fig. 5). The aggregates are often aligned into chains with an orientation that may potentially be controlled by muscovite surface structure, although this requires further study. The width of the aggregates measured along the shortest cross section is 64–200 nm and averages 78 nm. Their heights range from 1.3 to 6.8 nm and average 3.9. Attempts to image at smaller scan sizes (i.e., greater magnification) resulted in removal and smearing of the particles. This is a common problem when imaging soft and easily deformed surfaces (Radmacher et al., 1992). In the middle of Figure 5 is an area (~2 × 2 μm) where particles were removed by imaging before zooming out, suggesting low adsorption affinity at pH 6.

To test the effects of increased concentration of organic carbon, we performed experiments at pH 5, in 0.01 mol/L $CaCal_2$, and with ~100 mgC L^{-1} XAD-8 isolate. As shown in Figure 6 and reported by Maurice and Namjesnik-Dejanovic (1999), at this high concentration, the NOM forms ring-shaped aggregates with average diameter of 49.1 ± 9.7 nm. The interannular spacings on many of these rings contain smaller rings with pore spaces < 10 nm. Some of the larger rings consist of coalesced spheroids with diameter < 5 nm. Higher resolution images are required to probe the details of the ring structure. According to Israelachvili (1995) polymeric materials can assume a "torus" shape if the two ends of a rod-like aggregate bend and join together. We believe that the ring shape is more likely related at least in part to lateral interactions between neighboring NOM molecules at high NOM sorption densities, because spheres rather than rings were observed at lower concentrations (Fig. 5, above).

One explanation for this structure might be related to the biologic origins of HS. Goodenough and Heuser (1985) published TEM images of a cross section through the cell of an alga, *Chlamidomonas reinhardi*. The outer layers of the cell wall (particularly a layer known as the W6 layer) had a structure morphologically very similar to what we observed for the sorbed NOM. Moreover, Goodenough and Heuser (1985) showed that when the W6 portion of the cell was extracted with 1 mol/L perchlorate, and dialyzed against water, the fragments reassembled into an array of rings identical to the original structure. In a similar study on nucleated assembly of W6 glycoproteins, Adair et al. (1987) suggested that all the information required for the assembly of the crystalline layer resides in its molecular constituents. The compounds they studied represent major cell-wall components of dicotyledonous plants (plants with two-seed leaves) and of many algae. It is possible that NOM maintains at least some of the structure of its biologic precursors, and that self-assembly occurs when the conditions are favorable, such as when a nucleating surface is provided. This is an hypothesis which appears to warrant future investigation.

Figure 7a is an example of an image obtained at pH 8 (100 mgC L^{-1}) of surface water XAD-8 extract in 0.001 mol/L $CaCl_2$ with pH adjusted to 8 using NaOH. Diagonal lines running from the lower left to the upper right in these images are steps on the mica surface, due to imperfect cleavage. No

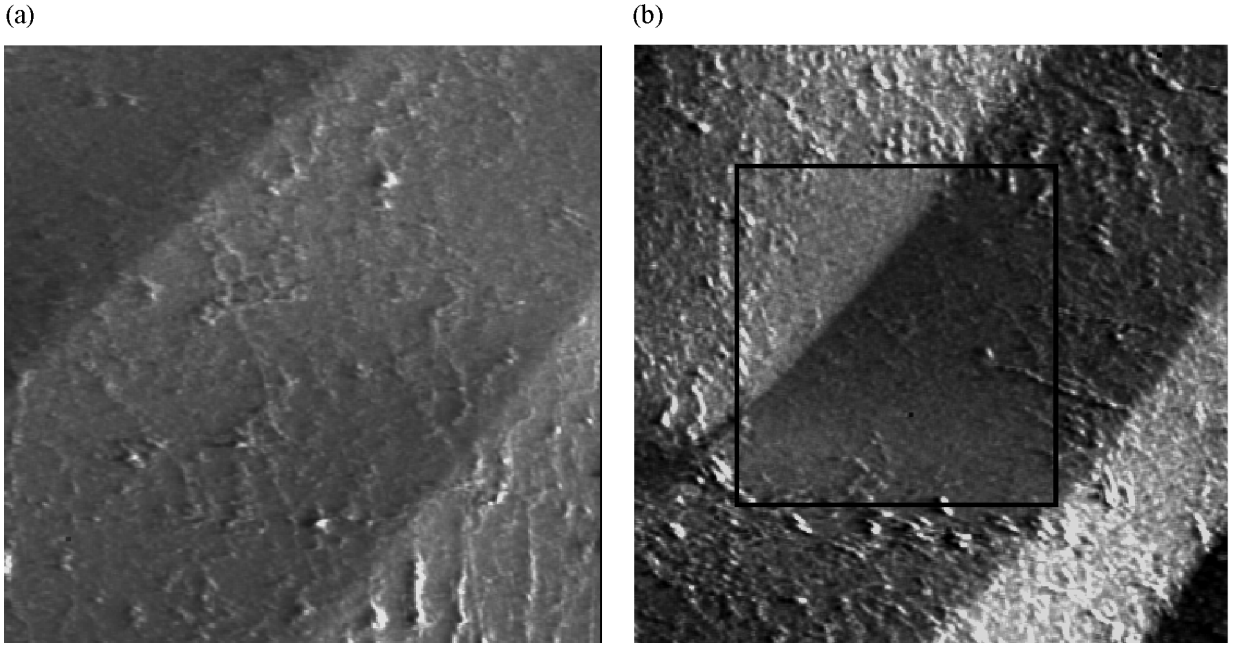

Fig. 7. (a) Amplitude mode image of surface water XAD-8 isolate on muscovite in 0.001 mol/L $CaCl_2$ at pH 8. (b) When an area of the surface was imaged repeatedly at small scan size (see area delineated by a box), the NOM was removed from the surface by tip-sample interactions during scanning. Upon zooming out, NOM gradually began to reappear in this area. (a) 4 μm, (b) 4.5 μm on a side. Horizontal streaks are scan-related artifacts.

preferential NOM sorption was observed along these steps. The surface was difficult to image, and NOM particles were easily moved by the tip. In some places, spherical particles are present. In other places, linear or chain-like structures consisting of aligned spherical particles can be seen. Although some structures may be artifacts, we believe that most of these linear structures are 'real' rather than drag marks caused by a single spherical particle pushed along the surface by the tip. Most structures were reproducible on subsequent scans.

Chain height ranges from 0.6 to 2.7 nm and averages 1.5 nm. Width varies considerably, especially where several chains are joined together. Measurements on an apparent single chain showed that average width (x-y) was 52.5 nm. Again, similar to experiments at pH 6, attempts to image with better resolution, i.e., smaller areas, resulted in removal and smearing of particles. In the central portion of Figure 7b is an area ($\sim 2 \times 2$ μm) where NOM was removed by repeated imaging before zooming out. It is obvious that linear NOM aggregates are reappearing in the cleaned area, particularly near the right side.

Figure 8 is an image of a sample in which 50 mgC L^{-1} muck fulvic acid was used with pH adjusted to 11 with NaOH, and no other electrolyte. A regular array of fine linear features, each 0.2–4.0 nm high and $\sim$ 6.4 nm wide, appears. This image is at first puzzling because it is known from batch experiments that NOM sorption substantially decreases as pH increases (Tipping and Cook, 1982; Ochs et al., 1994). The highly ordered structures are probably not NOM aggregates, but NOM may be a necessary component for their formation. They are more robust than other NOM structures as they are not as easily eroded by the tip upon scanning. We did not observe these structures in inorganic pH 11 NaOH solutions.

There is a striking morphologic similarity between these structures and recently reported silica-surfactant tubules which assembled on muscovite, graphite, and amorphous silica surfaces in the presence of dissolved Si and organic surfactants and were imaged by SEM, TEM, and AFM (Aksay et al., 1996; Yang et al., 1996; Velev et al., 1998). In our experiments at pH 11, the first few hours of imaging revealed only a typical mica

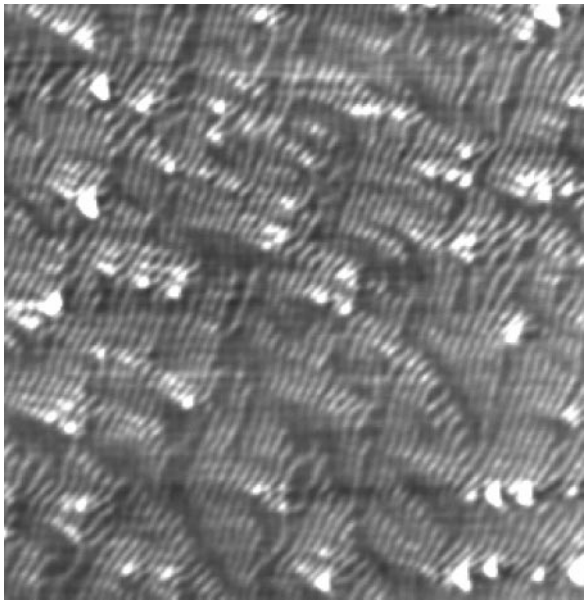

Fig. 8. Height mode image of highly ordered structures on mica at pH 11. We hypothesize that the mica surface restructured most probably due to Si dissolution and reprecipitation, in the presence of NOM. 250 nm on a side.

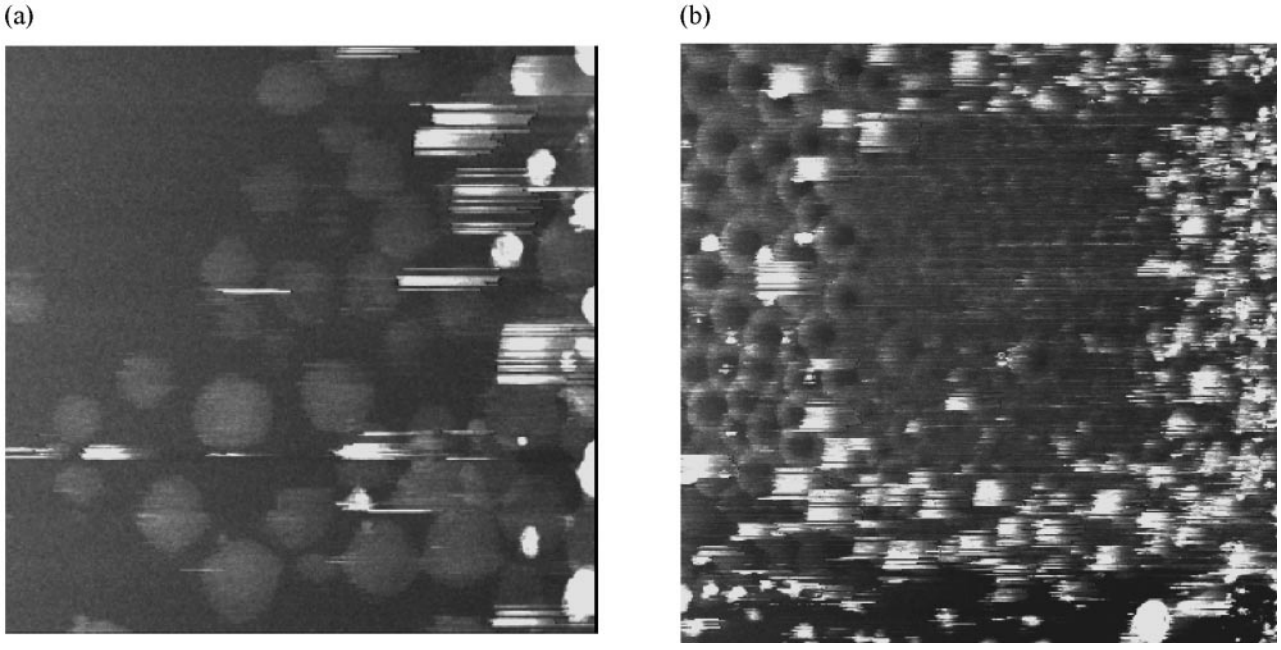

Fig. 9. (a) Flattened spherical aggregates of groundwater NOM imaged on hematite with light tapping; the underlying surface cannot be seen but is similar to (b), which contains flattened disk or ring-shaped aggregates (a) 3.5 μm, (b) 3.2 μm on a side.

surface, with some small dissolution pits. The structures shown in Figure 8 appeared after the system sat for 6 h. We therefore hypothesize that the dissolution of mica at high pH released Si (Brady and Walther, 1989) which then interacted with NOM to form a surface precipitate or rearranged layer that was perhaps templated by the NOM and/or the underlying mica. This hypothesis is consistent with observations by Linares and Huertas (1971; reconfirmed by K. Nagy, U. Colorado, Boulder, pers. commun.) that NOM enhances kaolinite formation at low temperature, in that NOM appears to have the ability to influence (alumino)-silicate secondary phase formation. Recently, Kinrade et al. (1999) showed that addition of aliphatic polyols (poly-hydroxy alcohols) to aqueous silicate solutions yielded stable hypervalent silicate anions in the form of polyolate complexes with silicon in either 5- or sixfold coordination with oxygen. They thus hypothesized that organic molecules and surfaces with polyhydroxy groups may isolate silica and silicic acids in nature. This is consistent with our preliminary interpretation of images such as the one shown in Figure 8. Our results thus suggest that NOM may play an important role in phyllosilicate diagenesis.

The range of structures observed under different conditions on muscovite indicates that simple models of NOM sorption clearly are not adequate to understand NOM interactions with mineral surfaces. For example, the Langmuir model, which assumes monolayer adsorption and no lateral interactions between molecules (e.g., Sposito, 1989), clearly does not correctly reflect NOM sorption mechanisms. The term 'monolayer' adsorption is likely not appropriate to describe the complex, 3-dimensional, often aggregated structures of sorbed NOM. Hence, while the Langmuir model is simple to apply, it likely obscures details of NOM sorption mechanisms. As a second example, a variety of different models have been proposed to account for NOM conformations and effects of conformations on sorption. Au et al. (1999) recently discussed a linear polyelectrolyte model wherein NOM chains attach to a surface with some tails and loops extending into solution. While some of our data (e.g., Fig. 7) suggest that NOM may adsorb as linear, flexible polyelectrolytes under certain conditions, other types of conformations and aggregate structures (e.g., single-molecule spheres, spherical aggregates, toroidal structures) clearly need to be considered.

3.2. Imaging on Hematite

Hematite was chosen as an additional substrate because Fe(III)(hydr)oxides are ubiquitous in subsurface environments, often forming coatings on other grains, and because NOM generally sorbs strongly to the hematite surface, especially at acidic pH (e.g., Gu et al., 1994; Maurice et al., 1998). Since the surface of natural hematite is rough at the nanometer scale, it was impossible to distinguish small NOM particles such as those imaged on mica. On the other hand very strong attraction of NOM for the hematite surface resulted in sorption of "multi layered" aggregates. We imaged a sample of groundwater NOM. When the z-scan size was kept large and the tapping conditions were kept light, layers of flattened spherical aggregates appeared, an example of which is shown in Figure 9a. There is an underlying layer of ring- or disk-shaped structures (Fig. 9b) that cannot be seen in this image because the computer program cannot display a high-relief surface easily as a single printable image. The brightest parts of the image represent the highest (closest to the scanning probe) NOM aggregates, which are flattened spherical structures (overall external

shape) that are partially destroyed by repeated scanning. Their x-y diameter varies between 200 and 500 nm. Prolonged imaging in one area causes these aggregates to be swept aside.

Figure 9b shows an area which was imaged several times so that many of the large aggregates shown in 9a were removed, and the lower layer can be seen more easily. There is a highly ordered structure of "torus- like" aggregates on top of which are some remaining (partially damaged by probe) spherical aggregates. It is apparent that flattened spherical aggregates change to either a disk-like or "torus" shape (we cannot distinguish which) when moved closer to the surface and packed tightly together. Strong surface attraction exerted by the underlying hematite surface and lateral interactions between aggregates packed closely together may contribute to the disk- or torus-like shape. The average outer diameter of the aggregates is 800 to 1000 nm measured in the x-y-direction. Because of the uneven surface and noise on the height images, the height of these aggregates is difficult to determine.

At the present time, we do not know the detailed chemical properties and structures of the large, spherical aggregates. However, their morphology suggests that they could potentially have a micelle-like structure. Comparison of these large aggregates with recently published AFM images of poly(butadiene-block-2-vinylpyridene) micelles on highly oriented pyrolitic graphite (HOPG, Regenbrecht et al., 1999) shows similar shapes and layering of micelles. Moreover, images of the same block copolymer on mica, described as vesicles (Regenbrecht et al., 1999, Figs. 3b and 4b), show structure and dimensions similar to what we described as rings in Figure 6 and torus-like structures in Figure 8b, respectively. Based on surface tension measurements, Rochus and Sipos (1978) and Phi and Wasowski (1984) hypothesized that humic acid reaches critical micellar concentration at concentration above 1%. But more than one critical micelle concentration should be expected since NOM is a complex mixture of compounds (Hayase and Tsubota, 1983). Moreover, effects of trivalent cations on micelle and aggregate formation need to be considered. It is possible that the strong attraction of NOM for the hematite surface resulted in a concentration gradient with relatively high NOM concentrations near the hematite surface. If so, then the NOM might have reached local concentrations high enough for micelles to form at or near the hematite surface, but not at the muscovite surface. If indeed NOM forms micelles, then this would agree with predictions by Wershaw (1992) and with observations of hydrophobic organic compounds partitioning (Schlautman and Morgan, 1993; Murphy et al., 1994, Piatt and Brusseau, 1998; Pignatello, 1998; Uhle et al., 1999). The NOM water sample used in this experiment has high Al and Fe concentrations, and these trivalent cations are well known to enhance NOM aggregation (Schnitzer and Khan, 1978; Alargova et al., 1998).

Our results agree well with in-solution X-ray microscope images of dissolved concentrated aquatic fulvic acid (0.1 g L^{-1} carbon) at pH 4 and in the presence of 0.001 mol/L Fe^{3+} (Myneni et al., 1999). Myneni et al. (1999) reported globular structures with mean diameter = 0.3 μm, along with thread-like structures. The globular structures we imaged (Fig. 9a) had similar shape and diameter. However, we did not observe thread-like structures.

4. SUMMARY AND CONCLUSIONS

Our results demonstrate that AFM can be used to image sorbed NOM at the molecular to aggregate scale. Major observations include:

1. In $CaCl_2$ and LiCl at pH 3, we observed "spherical" structures of size appropriate for single NOM molecules sorbed to the mica surface. Greater sorption density in $CaCl_2$ was consistent with previous observations of enhanced sorption in the presence of Ca. The observation of possible single NOM spherical molecules in $CaCl_2$ but aggregates of spherical molecules in LiCl suggests that the electrolytes affect interactions between NOM molecules. We did not succeed in obtaining stable images of NOM in NaCl at pH 3, although good images of the muscovite substrate were obtained. This is consistent with weak adsorption in the presence of NaCl.
2. At intermediate pH (5–6), in $CaCl_2$, and at relatively low NOM concentrations (20–50 mgC L^{-1}), on mica, we observed somewhat larger spherical structures which were likely NOM aggregates, perhaps small micelles. At higher NOM concentrations ($\sim$100 mgC L^{-1}), we observed ring-shaped or toroidal aggregate structures. The ring structures represent significant self-assembly which could have important implications regarding NOM genesis, structure and reactivity. Observation of potential micelle-like structures calls for further investigations of micellar models for NOM partitioning behavior.
3. At pH 8, in $CaCl_2$, on mica, imaging was especially difficult probably due to decreased sorption affinity with increased pH. Some spheres and linear aggregate structures were observed
4. At pH 11 (set with NaOH), and 50 mgC L^{-1} NOM concentration, highly ordered fine linear structures were observed on mica. We hypothesize that these structures represent reordering of the muscovite surface in the presence of NOM and as Si dissolves from the surface. Our observation suggests that NOM may play a role in phyllosilicate diagenesis.
5. On hematite at pH 4, a bulk (filtered but without NOM isolation) shallow ground-water sample with high natural Fe and Al concentrations showed a lower layer of flattened disk or ring-shaped structures and a second layer of spherical structures. These aggregates might have micelle-like structures, which suggests that further investigation of the effects of aggregate structure on HOC partitioning is warranted. Moreover, these images agree with new in-solution X-ray microscopy of high-Fe NOM containing solutions, verifying that the two techniques produce similar images.

We have reported initial observations of NOM sorption on muscovite under a variety of different conditions, along with preliminary work on hematite. Because conformations and aggregate structures may potentially be influenced by mineral surface properties, this study is presently being expanded to include additional minerals. Our results demonstrate that in-solution AFM is crucial for understanding NOM sorption. AFM is a direct observation method that may open numerous doors for new inquiry and investigation. AFM imaging is difficult and time consuming; hence, development of a com-

prehensive understanding of sorbed NOM conformations and aggregate structures will require a great deal of effort. Nevertheless, such direct observations are required to develop realistic models of NOM sorption and as a basis for further understanding of NOM reactivity.

Acknowledgments—We thank M. Pullin and G. Aiken for the XAD-8 extraction. We thank S. Cabaniss (KSU) for much helpful discussion. We thank the following colleagues for reviewing early drafts of this manuscript: J. Kubicki, J. Leenheer, S. Traina, and R. Wershaw. We thank M. Schlautman, R. Burruss and an anonymous reviewer for excellent review comments. This research was funded by the National Science Foundation, Hydrologic Sciences Division.

Associate editor: R. C. Burruss

REFERENCES

Adair W. S., Steinmetz S. A., Mattson D. M., Goodenough U. W., and Heuser J. E. (1987) Nucleated assembly of Chlamydomonas and Volvox cell-walls. *J. Cell Biol.* **105,** 2373–2382.

Aiken G. R., Brown P. A., Noyes T. I., and Pinckney D. J. (1994) Molecular size and weight of fulvic and humic acids from the Suwannee River. In *Humic Substances in the Suwannee River, Georgia: Interactions, Properties, and Proposed Structures* (eds. R. C. Averett, J. A. Leenheer, D. M. McKnight, and K. A. Thorn), USGS Water-Supply Paper 2373, pp. 89–98.

Aiken G. R., McKnight D. M., Thorn K. A., and Thurman M. (1992) Isolation of hydrophilic organic acids from water using nonionic macroporous resins. *Org. Geochem.* **18,** 567.

Aksay I. A., Trau M., Manne S., Honma I., Yao N., Zhou L., Fenter P., Eisenberger P. M., and Gruner S. M. (1996) Biomimetic pathways for assembling inorganic thin films. *Science* **273,** 892–898.

Alargova R. G., Ivanova V. P., Kralchevsky P. A., Mehreteab A., and Broze G. (1998) Growth of rod-like micelles in anionic surfactant solutions in the presence of Ca^{2+} counterions. *Colloid Surf. A.* **142,** 201–218.

Au K.-K., Penisson A. C., Yang S., and O'Melia C. R. (1999) Natural organic matter at oxide-water interfaces: Complexation and conformation. *Geochim. Cosmochim. Acta* **63,** 2903–2917.

Babcock K. L. and Prater C. B. (1991) *Phase Imaging: Beyond Topography*. (www.di.com)

Barrett R. C. and Quate C. F. (1991) High-speed. large scale imaging with the atomic force microscope. *J. Vac. Sci. Technol. B.* **9,** 302–306.

Bezanilla M., Bustamante C., and Hansma H. (1993) Improved visualization of DNA in aqueous buffer with the atomic force microscope. *Scan. Micro.* **7,** 1145–1148..

Brady P. V. and Walther J. V. (1989) Controls on silicate dissolution rates in neutral and basic pH solutions at 25°C. *Geochim. Cosmochim. Acta* **53,** 2823–2830.

Butt H. J. and Gerharz B. (1995) Imaging homogenous and composite latex particles with an atomic force microscope. *Langmuir* **11,** 4735–4741.

Chen Y. and Schnitzer M. (1989) Sizes and shapes of humic substances by electron microscopy. In *Humic Substances II* (eds. M. H. B. Hayes, P. MacCarthy, R. L. Malcolm, and R. S. Swift), pp. 621–638, Chap. 22. John Wiley and Sons Ltd.

Chin Y.-P., Aiken G., and O'Loughlin E. (1994) Molecular weight, polydispersity, and spectroscopic properties of aquatic humic substances. *Env. Sci. Technol.* **28,** 1853–1858.

Cornel P. R., Summers R. S., and Roberts P. V. (1986) Diffusion of humic acid in dilute aqueous solutions. *J. Colloid Interface Sci.* **110,** 149.

Dempsey B. A. and O'Melia C. R. (1983) Proton and calcium complexation of four fulvic acid fractions. In *Aquatic and Terestrial Humic Materials* (eds. R. F. Christman and E. T. Gjessing) pp. 239–273, Chap. 12. Ann Arbor Sci.

Digital Instruments Inc. (1996–97) MultiMode SPM Instruction Manual.

Ducker W. A., Senden T. J. and Pashley R. M. (1992) Measurement of forces in liquids using a force microscope. *Langmuir* **8,** 1831–1836.

Frommer J. (1992) Scanning tunneling microscopy and atomic force microscopy in organic chemistry. *Angew. Chem. Int. Ed. Engl.* **31,** 1298–1328.

Goodenough U. W. and Heuser J. E. (1985) The Chlamydomonas cell wall and its constituent glycoproteins analyzed by the quick-freeze, deep-etch technique. *J. Cell Biol.* **101,** 1550–1568.

Gu B., Schmitt J., Chen Z., Liang L., and McCarthy J. F. (1994) Adsorption and desorption of natural organic matter on iron oxide: Mechanisms and models. *Env. Sci. Tech.* **28,** 38–46.

Hansma P. K., Cleveland J. P., Radmacher M., Walters D. A., Hillner P. E., Bezanilla M., Fritz M., Vie D., and Hansma H. G. (1994) Tapping mode atomic force microscopy in liquids. *Appl. Phys. Lett.* **64,** 13, 1738–1740.

Israelachvili J. N. (1995) Intermolecular and Surface Forces. Academic Press.

Johnsson P. A., Eggleston C. M., and Hochella M. F. Jr. (1991) Imaging molecular-scale structures and microtopography of hematite with the atomic force microscope. *Am. Mineral.* **76,** 1442–1445.

Johnsson P. A., Hochella M. F. Jr, Parks G. A., Blum A. E., and Sposito. G. (1992) In *Proceedings of the 7th International Symposium on Water-Rock Interaction* (eds. Y. K. Kharaka and A. S. Maest), pp. 159–162. A.A. Balkema.

Johnsson P. A. and Barringer, J. L. (1993) Water Quality and Hydrogeological Processes in McDonalds Branch Basin, New Jersey Pinelands, 1984–88. USGS Water-Resources Investigation Report. 91-4081.

Junta J. and Hochella M. F. (1994) Manganese (II) oxidation at mineral surfaces - microscopic and spectroscopic study. *Geochim. Cosmochim. Acta* **58,** 4985–4999.

Kinrade S. D., Del Nin J. W., Schach A. S., Sloan T. A., Wilson K. L., and Knight C. T. G. (1999) Stable five- and six-coordinated silicate anions in aqueous solution. *Science* **285,** 1542–1545.

Langmuir, D. (1997) Aqueous Environmental Geochemistry. Prentice-Hall.

Leppard G. G., Burnison B. K., and Buffle, J. (1990). Transmission electron microscopy of the natural organic matter of surface waters. *Anal. Chim. Acta* **232,** 107–121.

Linares J. and Huertas F. (1971) Kaolinite: Synthesis at room temperature. *Science* **171,** 896–897.

Lord D. G., Barringer J. L., Johnsson P. A., Schuster P. F., Walker R. L., Fairchild J. E., Sroka B. N., and Jacobsen E. (1990) Hydrogeochemical Data From an Acidic Deposition Study at McDonalds Branch Basin in the New Jersey Pinelands, 1983–86. U.S.G.S. Open-File Report 88-500. p. 132.

Magonov S. N., Cleveland J., Elings V., Denley D., and Whangbo, M.-H. (1997a) Tapping-mode atomic force microscopy study of the near-surface composition of a styrene-butadiene-styrene triblock copolymer film. *Surf. Sci.* **389,** 201–211.

Magonov S. N., Elings V., and Whangbo M.-H. (1997b) Phase imaging and stiffness in tapping-mode atomic force microscopy. *Surf. Sci.* **375,** L385–L391.

Magonov S. N. and Reneker D. H. (1997) Characterization of polymer surfaces with atomic force microscopy. *Ann. Rev. Mat. Sci.* **27,** 175–222.

Markiewicz P. and Goh M. C. (1994) Atomic force microscopy probe tip visualization and improvement of images using a simple deconvolution procedure. *Langmuir* **10,** 5–7.

Maurice P. A., Hochella M. F. Jr, Parks G. A., Sposito G., and Schwertmann, U. (1995) Evolution of hematite surface microtopography upon dissolution by simple organic acids. *Clays Clay Miner.* **43,** 29–38.

Maurice P. A., Namjesnik-Dejanovic K., Lower S., Pullin M., Chin Y.-P., and Aiken G. R. (1998) Sorption and fractionation of natural organic matter on kaolinite and goethite. In *Water Rock Interaction* (eds. G. B. Arehart and J. R. Hulston), pp. 109–113. Balkema.

Maurice P. A. and Namjesnik-Dejanovic K. (1999) Aggregate structures of sorbed humic substances observed in aqueous solution. *Env. Sci. Tech.* **33,** 1538–1541.

Maurice P. and Lower S. K. (1998) Using atomic force microscopy to study soil mineral reactions. *Adv. Agron.* **62,** 1–43.

McCarthy J. F. and Jimenez B. D. (1985) Interactions between poly-

cyclic aromatic hydrocarbons and dissolved humic material: Binding and dissolution. *Env. Sci. Tech.* **19,** 1072–1076.
Meier M., Namjesnik-Dejanovic K., Maurice P. A., Chin Y.-P., Aiken G. R. (1999) Fractionation of aquatic natural organic matter upon sorption to goethite and kaolinite. *Chem. Geol.* **157,** 275–284.
Mertig M., Klemm D., Pompe W., Zanker H., and Bottger, M. (1999) Scanning force microscopy of spin-coated humic acid. *Surf. Interface Anal.* **27,** 426–432.
Murphy E. M., Zachara J. M., and Smith S. C. (1990) Influence of mineral-bound humic substances on the sorption of hydrophobic organic compounds. *Env. Sci. Tech.* **24,** 1507–1516.
Murphy E. M., Zachara J. M., Smith S. C., Phillips J. L., and Wietsma T. W. (1994) Interaction of hydrophobic organic compounds with mineral-bound humic substances. *Env. Sci. Tech.* **28,** 1291–1299.
Myneni S. C. B., Brown J. T., Martinez G. A. and Meyer-Ilse W. (1999) Imaging of humic substance macromolecular structures in water and soils. *Science* **286,** 1335–1337.
Namjesnik-Dejanovic K. and Maurice P.A. (1997) Atomic force microscopy of soil and stream fulvic acids. *Colloid Surf. A.* **120,** 77–86.
Namjesnik-Dejanovic K, Maurice P. A., Aiken G. R., Cabaniss S. E., Chin Y.-P., and Pullin M. J. (2000). Adsorption and fractionation of a muck fulvic acid on kaolinite and goethite at pH 3.7, 6 and 8. *Soil Sci.* **165,** 545–559.
Ochs M., Cosovic B., and Stumm W. (1994) Coordinative and hydrophobic interaction of humic substances with hydrophilic Al_2O_3 and hydrophobic mercury surface. *Geochim. Cosmochim. Acta* **58,** 639–650.
Piatt J. J. and Brusseau M. L. (1998) Rate-limited sorption of hydrophobic organic compounds by soils with well-characterized organic matter. *Env. Sci. Tech.* **32,** 1604–1608.
Pignatello J. J. (1998) Soil organic matter as a nanoporous sorbent of organic pollutants. *Adv. Colloid Inter. Sci.* **76–77,** 445–467.
Putman C. A. J., Van der Werf K. O., De Groth B. G., Van Hulst N. F., and Greve J. (1994) Tapping mode atomic force microscopy in liquid. *Appl. Phys. Lett.* **64,** 2454–2456.
Radmacher M., Tillmann R. W., Fritz M., and Gaub H. E. (1992) From molecules to cells: Imaging soft samples with the atomic force microscope. *Science* **257,** 1900–1905.
Schimpf M. E. and Petteys M. P. (1996) Characterization of humic materials by flow field-flow fractionation. *Colloid Surf. A.* **120,** 87–100.
Schlautman M. A. and Morgan J. J. (1993) Binding of a fluorescent hydrophobic organic probe by dissolved humic substances and organically-coated aluminum oxide surface. *Env. Sci. Tech.* **27,** 2523–2532.
Schnitzer M. and Khan S. U. (1978) Soil Organic Matter. Elsevier.
Siedlecki C. A., Lestini B. J., Kottke-Marchant K., Eppell S. J., Wilson D. L., and Marchant R. E. (1996) Shear-dependent changes in the three-dimensional structure of human von Willebrand factor. *Blood.* **8,** 2939–2950.
Sposito G. (1989) The Chemistry of Soils. Oxford University Press.
Stevenson I. L. and Schnitzer M. (1982). Transmission electron microscopy of extracted fulvic and humic acids. *Soil Sci.* **133,** 179–185.
Stumm W. and Morgan J. J. (1996) Aquatic Chemistry, 3rd Edition. John Wiley & Sons.
Tipping E. (1981) The adsorption of aquatic humic substances by iron oxides. *Geochim. Cosmochim. Acta* **45,** 191–199.
Tipping E. and Cook D. (1982) The effects of adsorbed humic substance on the surface charge of goethite (α-FeOOH) in freshwaters. *Geochim. Cosmochim. Acta* **46,** 75–80.
Uhle M. E., Chin Y.-P., Aiken G. R., and McKnight D. M. (1999) Binding of polychlorinated biphenyls to aquatic humic substances: The role of substrate and sorbate properties on partitioning. *Env. Sci. Tech.* **33,** 2715–2718.
Velev O. D., Jede T. A., Lobo R. F., and Lenhoff A. M. (1998) Microstructured porous silica obtained via colloidal crystal templates. *Chem. Mater.* **10,** 3597–3602.
Wershaw R. L. (1992) Membrane-micelle model for humus in soils and sediments and its relation to humification. *USGS Open-File Report. 91-513.*
Wilson D. L., Dalal P., Kump K. S., Benard W., Xue P., Marchant R. E., and Eppell S. J. (1996) Morphological modeling of atomic force microscopy imaging including nanostructure probes and fibrinogen molecules. *J. Vac. Sci. Technol. B.* **14,** 2407–2415.
Yang H., Kuperman A., Coombs N., Mamiche-Afara S., and Ozin G. A. (1996) Synthesis of oriented films of mesoporous silica on mica. *Nature* **379,** 703–705.
Yokoyama A., Srinivasan K. R., and Fogler H. S. (1989) Stabilization mechanisms by acidic polysaccharides. Effects of electrostatic interactions on stability and peptization. *Langmuir* **5,** 534–538.
Zhou, Q., Cabaniss, S.E., and Maurice, P.A. (2000) Considerations in the use of high-pressure size exclusion chromatography (HPSEC) for determining molecular weights of aquatic humic substances *Water Res.* **34,** 3505–3514.
Zhou Q., Maurice P. A., and Cabaniss S. E. (in press) Adsorption and fractionation of natural organic matter reaction (NOM) on goethite: Equilibrium and kinetic studies. *Geochim. Cosmochim. Acta*.